Novel folded pendulum residual seism accelerometer for the Virgo gravitational wave observatory: parasitic resonance mode characterisation

Harun Džafić
National Institute for Subatomic Physics, Nikhef, Amsterdam
dzafic.h@hotmail.com

ABSTRACT

Optical components of a gravitational wave (GW) detector must both actively and passively be isolated from microseisms to be able to detect GWs. Active attenuation is achieved by making use of accelerometers within seismic isolation systems. Herein, a characterisation of the internal leg mode resonances of an improved design Folded Pendulum accelerometer, present at the Virgo GW observatory, is being discussed. We model internal leg mode resonances of the accelerometer using Finite Element Method analysis and we experimentally confirm the horizontal in-plane and tilt resonances below 1 kHz, by use of a shadow sensing application combined with Bode plots.

Keywords
Gravitational waves, seismic isolation, Virgo gravitational wave observatory, accelerometer, shadow sensing.

INTRODUCTION

Gravitational waves (GWs) have been predicted by Albert Einstein as part of his general theory of relativity and have recently been discovered experimentally by GW observatories LIGO and Virgo [1, 2]. Combining GW observations with electromagnetic spectroscopic measurements allows for much better identification, characterization and understanding of the physical and astronomical processes involved in a GW event, which typically is a black hole or neutron star binary system merging.

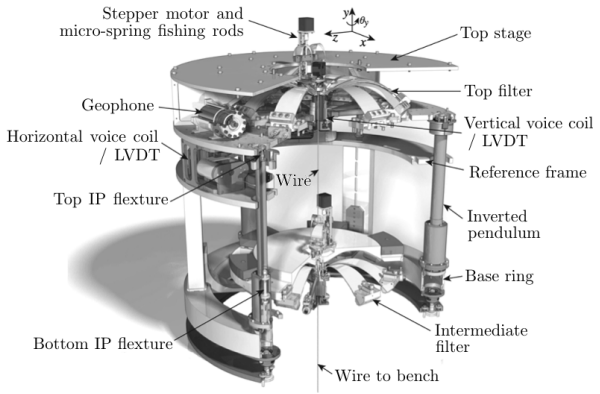

Figure 1: MultiSAS design: passive and active attenuation is achieved by chaining pendulums and measuring residual motion with geophones on the top stage, respectively. [5]

The National Institute for Subatomic Physics (Nikhef) in the Netherlands is concerned with research on aspects of fundamental physics such as gravitational waves, dark matter and elementary particles. It takes part in the Virgo-project: a partnership of multiple European countries that operate the Virgo GW detector in Cascina, Italy [3]. Amongst other devices, Nikhef has designed and built MultiSAS, a multiple-stage 6 degree of freedom seismic attenuation system (SAS). Five of these systems are used to isolate the optical tables which house the alignment and photo-detection optics at the Virgo GW detector. Horizontal vibrations of MultiSAS' top stage are currently being measured with geophones in order to actively attenuate these vibrations. Because these geophones have a low sensitivity below 0.2 Hz, a new horizontal low-frequency Folded Pendulum accelerometer (FPA) is being worked on as a replacement. The latter is a mechanical oscillator consisting of a normal pendulum (NP), an inverted pendulum (IP) and a freely moving mass. The displacement of this moving mass is measured with a linear variable differential transformer (LVDT) and its position can be actuated by a voice coil actuator (VCA). The accelerometer can be operated in two modes: open and closed loop, in which the sensor outputs are obtained from the LVDT and VCA signals, respectively. The control bandwidth of the FPA is limited because of unwanted resonances, so-called parasitic resonances, which are ascribed to its internal vibrational modes, in particular of the pendulum legs. Therefore, the incentive of this study lies to characterize the redesign of the FPA with higher pendulum leg mode frequencies. This characterisation consists of a Finite Element Method (FEM) analysis and a shadow sensing application, the combination of which will show whether or not the redesign has resulted in a broader bandwidth. The shadow sensor measurements will ultimately provide a better understanding of the mode behavior, which will result in new insights on how to improve the accelerometer as a whole (mainly its brownian noise level reduction due to finetuning the flexure dimensions) and its bandwidth specifically. It is clear that understanding the resonance modes is the first step towards a whole new era of achieving better active attenuation for MultiSAS.

MULTISAS AND ACCELEROMETER MECHANICS

MultiSAS attenuates the horizontal residual seismic motion of an optical bench down to 10^{-15} m/$\sqrt{\text{Hz}}$ for frequencies above 10 Hz [4] based on passive attenuation. This optical bench contains instruments for the interferometers alignment. A conceptual sketch of MultiSAS is shown in Figure 1. It contains three IP legs to support and isolate the top stage. Both the top and the intermediate filter are geometric anti-spring

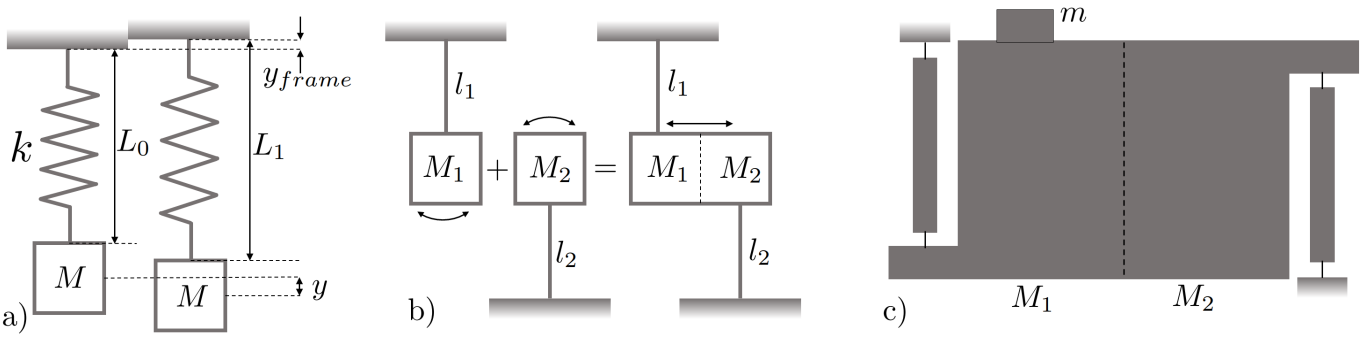

Figure 2: a) A mass-spring system attached to a frame, with spring constant k and mass M. The schematic on the left shows the system in equilibrium, whereas the other schematic shows the same system after a frame displacement. b) A schematic drawing of a simple folded pendulum with masses M_1 and M_2 and lengths l_1 and l_2. c) A schematic view of a realistic FP with thin and flexible joints. A small tuning mass m is present. [6]

(GAS) filters, which provide vertical attenuation to the optical bench. Figure 1 also shows sensors, namely LVDTs and geophones that measure the residual seismic movement of the top stage. They are necessary in order to correctly position the top stage, and in turn the bench, while also to sense the residual motion in order to damp the pendulum chain resonances and control its motion below a few Hz. The geophones have a low sensitivity below 0.2 Hz and the LVDTs measure displacements relative to the surrounding reference frame. The MultiSAS would benefit from an absolute (inertial) displacement sensor with a higher sensitivity at low frequencies and a broader bandwidth.

The key element in any inertial sensor is a mechanical oscillator similar to the simple mass-spring system as illustrated in Figure 2a). By solving the transfer function between the amplitude of a displacement sensor and the frame acceleration or displacement, one obtains harmonic oscillator-like equations, in which a low resonance frequency gives a better low frequency responsivity. A low frequency harmonic oscillator can be obtained by combining an NP with an IP, according to Figure 2b). Such a mechanism is called a folded pendulum (FP). The spring contribution of the NP is $k_1 = M_1 g/l_1$, whereas the spring contribution of the IP is $k_2 = -M_2 g/l_2$. The total spring contribution k of the FP is $k = k_1 + k_2$. Knowing that $\omega_0^2 = k/(M_1 + M_2)$ gives the resonance frequency for the simple-model FP as

$$\omega_0^2 = \frac{g}{M_1 + M_2}\left[\frac{M_1}{l_1} - \frac{M_2}{l_2}\right], \qquad (1)$$

which can be tuned as low as one wishes. However, this is a description of the FP in a simple form. The pendulum legs can be connected to thin elastic flexible joints (flexures), which are normally thickened to make them stiff and shifted apart with a main mass in between them to keep the main mass rotation to a minimum and essentially only allow the main mass to move horizontally. This main mass is constructed in such a way that its weight is equally distributed across both pendulum legs. Since this distribution is fixed, a small movable mass is added such that this mass distribution can be tuned. All of this would result in an FP as shown schematically in Figure 2c). By adding the spring contributions of the flexures k_{flex} and setting $l_1 = l_2 = l$, the resonance frequency becomes

$$\omega_0^2 = \frac{k_{flex} + (M_1 - M_2)g/l}{M_1 + M_2 + m}. \qquad (2)$$

Note that equation (2) does not contain any information on the position of the tuning mass m, but M_1 and M_2 are left as dependent on the position of m. Shifting m results in changing the weight suspended on the IP and NP, which changes the difference $M_1 - M_2$ in equation (2) and in turn ω_0. Using the Lagrangian method the FP can be described with the effects of the pendulum leg masses, their moments of inertia and more effects of the flexures [7, 8]. A picture of the FPA is shown in Figure 3.

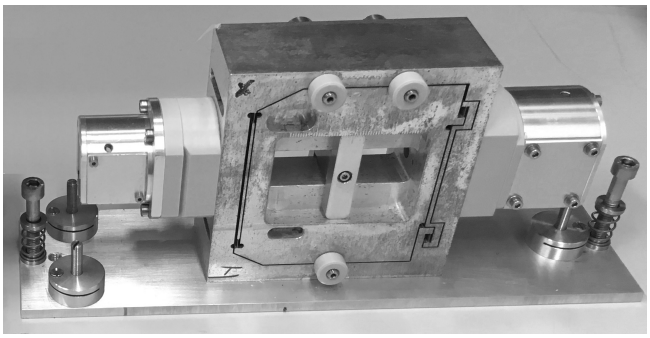

Figure 3: A picture of the new design FPA on a mounting plate, with the enclosures on the left and right being the housings of the LVDT and VCA, respectively.

PENDULUM LEG MODES AND SHADOW SENSING

Both pendulum legs of the FPA are connected to the moving mass and to the frame with four flexures for each leg. The eigenfrequencies of the legs are simulated with a Finite Element Method (FEM) along with an analytical verification using a simple geometry and assuming that the legs are rigid bodies. As mentioned before, low frequency in-plane leg modes (<1000 Hz) give unwanted resonances in the FPA's responsivity, limiting its bandwidth.

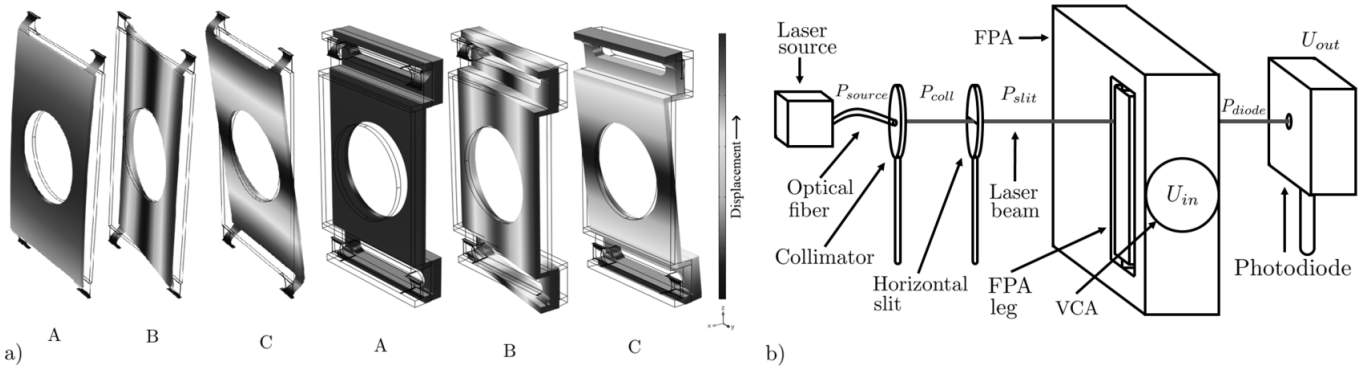

Figure 4: a) The NP (left) and IP (right) mode shapes b) Schematic implementation of the shadow sensor measurement technique on the FPA setup.

COMSOL Multiphysics has been used for modeling the three lowest eigenfrequencies for each leg. The three lowest frequency mode shapes for the NP and IP legs are displayed in Figure 4a). Mode A is the horizontal in-plane translation mode, where the leg moves back and forth in the same plane as the moving mass. The NP leg slightly banana-bends due to its thin geometry. Mode B is called the yaw mode, in which the leg rotates about its width whilst mode C is called the tilt mode, in which the leg rotates about its length. The FEM analysis also gives the frequencies for these modes, as seen in table I. In this case, analytic frequencies are determined as well.

Table I: The analytic and COMSOL mode frequencies for the new design FP with 100 μm flex thicknesses.

	IP			NP			
	A	B	C	A	B	C	
FEM	174.3	244.9	217.7	241.5	392.2	460.5	Hz
Analytic	161.9	235.4	224.0	266.1	428.2	435.4	Hz

The leg modes can be determined experimentally by use of a shadow sensing technique, which is shown schematically in Figure 4b). One may measure the transfer function of the two voltage signals to obtain

$$H(\omega) = \frac{U_{out}(\omega)}{U_{in}(\omega)} = \frac{\beta R G \varepsilon_{slit} \varepsilon_{coll} P_{source}}{M} \frac{\varepsilon_{leg}(\omega)}{\ddot{X}(\omega)}, \quad (3)$$

in which the $\varepsilon_{leg}(\omega)/\ddot{x}(\omega)$ term is the fraction of optical power blocked by the pendulum leg per unit of VCA acceleration. The leg mode will be excited by the voice coil at its resonance frequency, which would result in a peak in $|H(\omega)|$. Comparing $\arg(H(\omega))$ for the top and bottom part of the leg, one can deduce which mode shape corresponds to the peak.

RESULTS

The shadow sensor measured the displacements of the top and bottom part of the FPA legs, which uncovered the leg mode symmetries. The Bode plots for the IP and NP are shown in Figures 5. Specifically, there are three IP leg modes labeled A, B and C. Unlabeled artifacts occur in an inconsistent manner between the top and bottom measurement, suggesting that these perturbations arise from picked up accelerations. The measured leg mode frequencies agree with FEM and analytical calculations for a flex thickness of approx. 100 μm. Mode symmetries can be obtained with the phase information of Figure 5. The phase of mode A (which was measured at 161.25 Hz) indicates that the top and bottom part of the IP leg move in phase, thus confirming its FEM mode shape from Figure 4a). The phase of mode C (measured to be at 204.0 Hz) shows that the top and bottom part of the IP leg are moving out of phase, which also confirms its FEM mode shape. Yet, mode B (measured at 227.0 Hz), demonstrates that the top and bottom part do not share the same phase, which is inconsistent with the FEM mode shape. This inconsistency may be due to unequal laser alignments with respect to the leg itself, between the top and bottom measurements. The phases between top and bottom at this mode will be of opposite sign if the laser strikes the leg in the front for the top measurement and in the back part for the bottom measurement.

Similar results are shown for the NP. The top and bottom of the leg are in and out of phase for mode A (measured to be at 241.0 Hz) and C (426.25 Hz), respectively, which confirm the FEM mode shape. Mode B did not appear clearly during this measurement, possibly again due to this mode being overly sensitive to laser alignment. According to FEM and analytical calculations, that mode is expected just before the mode C frequency. This range shows two peaks, but the frequency shifts between the top and bottom of the peaks are too high to conclusively deduct which one of these stands for mode B, or even if any of these peaks actually *is* caused by mode B. A different implementation of the shadow sensor would be to shoot the laser parallel to the length of the leg, aiming to uncover mode B for both legs. The frequencies between the three different methods of calculating or measuring them are in good agreement within acceptable (experimental) error. This error is mainly caused due to the high frequency-dependency of the flexure thickness ($\propto t^{3/2}$) and a few assumptions in the equations and in the geometry of the FEM model, which are expected to be somewhat different than the physical system. Besides, the physical system also has production tolerances of the FPA, which results in inconsistent flexure thicknesseses, changing each mode frequency in an inconsistent manner. The

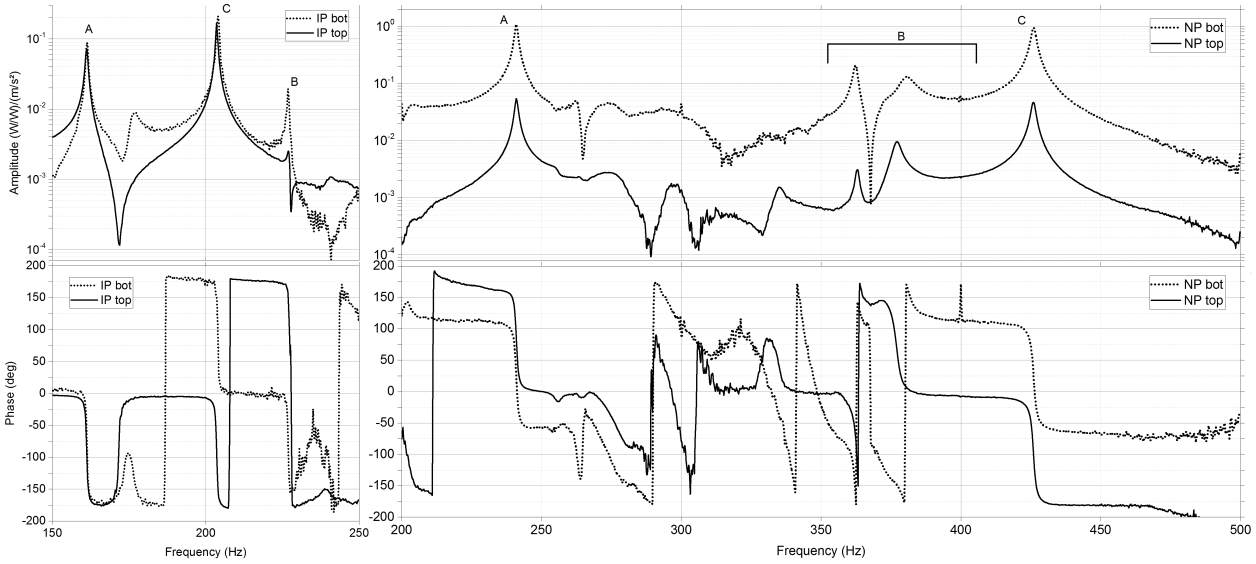

Figure 5: The shadow sensor Bode plot for $\varepsilon_{leg}(\omega)/\ddot{X}(\omega)$ (equation (3)) on the top and bottom (legend: bot) parts of the pendulum legs, averaged approx. 150 times. The annotations A, B and C stand for the mode shapes as discussed in Figure 4a). The FPA was actuated with a sine chirp. The spectral resolution is 0.25 Hz.

redesign of the FPA has shown to be successful as its bandwidth is considered to be the frequency of the first mode in the spectrum, which was 161.25 Hz.

CONCLUSIONS

FEM analysis corroborates that both pendulum legs have three resonance modes below 1 kHz. These have been shown to be a horizontal in-plane translation, yaw and tilt mode. The horizontal in-plane translation and the tilt mode have been confirmed experimentally by employing a shadow sensor measurement technique. It was not possible to confirm the yaw mode with the implemented shadow sensor measurement method, because this mode is prone to give inconsistencies in the phase information of the Bode plot with small changes in laser alignment. Both FEM, analytic and experimental frequencies exhibit somewhat similar values within the FPA production tolerances and FEM/analytic assumptions or simplifications. The leg mode frequencies have upshifted with respect to the previous design FPA, which means that its control bandwidth has broadened. The bandwidth therefore coincides more with the high responsivity frequency range of the Virgo GW detector, which improves this responsivity due to better attenuation in this frequency range. The bandwidth of the new design FPA has shown to be twice as broad as its previous design, meaning that the redesign has been effective.

OUTLOOK

A future perspective for the FPA is to apply shadow sensing in the length of the pendulum legs to be able to characterize the yaw mode. Mounting the shadow sensing setup on an optical rail or table and adding a translational stage will allow for improvements in laser alignment and obtaining more information from the amplitude of the Bode plots as a function of the leg coordinates (mainly its height). This will eventually result in a graphical representation of the leg mode shape and it will reveal detailed information about the (individual) flexure thicknesses and thereby the Brownian noise levels of the mechanics. Once this is obtained, one may continue with finetuning the design to achieve any goal a specific design may be set for. This goal may be a broad-bandwidth version of the FPA, a low Brownian noise level version or a combination of these two and other specific features. Any kind of optimization is possible, which means that the seismic attenuation will not be one of the restricting noises in Virgo's responsivity curve.

ROLE OF THE STUDENT

This paper is based on the thesis which the author has submitted for his graduation project while studying Applied Physics at the Fontys University of Applied Sciences in Eindhoven. His school and institute supervisors were Dr. Willem-Jan van Harskamp and Drs. Eric Hennes, respectively. All shown results were obtained and analyzed by the author himself.

REFERENCES

[1]A. Einstein, "Die Grundlage der allgemeinen Relativitätstheorie," Annalen der Physik, 1916.
[2]The LIGO Scientific Collaboration, The Virgo Collaboration, Phys. Rev. Lett. 119 161101 (2017)
[3]"Virgo". nikhef.nl. retrieved on 17 Oct 2017 from https://www.nikhef.nl/programma/virgo/.
[4]Verhaar, Sjors. "Characterisation of the use of two lasers in a monolithic accelerometer with an interferometric readout" (2013). Universiteit van Amsterdam. page 8, 16 & 17.
[5]F. Acernese et al. "Advanced Virgo: a second-generation interferometric gravitational wave detector" (2014). Page 44.
[6]Nikhef (2017), internal communication.
[7]Liu, Jiangfeng, Li Ju and David G. Blair. "Vibration isolation performance of an ultra-low frequency folded pendulum resonator". Physics Letters A 228.4 (1997) pages 243 - 249.
[8]Bertolini, Alessandro. "High sensitivity accelerometers for gravity experiments" (2001). Doktora Tezi, Università di Pisa. Page 2-8, 62-70 & 85.